PHYSICAL REVIEW B **94**, 134516 (2016)

Nuclear magnetic relaxation rates of unconventional superconductivity in doped topological insulators

Yuki Nagai
CCSE, Japan Atomic Energy Agency, 178-4-4, Wakashiba, Kashiwa, Chiba, 277-0871, Japan

Yukihiro Ota
Research Organization for Information Science and Technology (RIST), 1-5-2 Minatojima-minamimachi, Kobe, 650-0047, Japan
(Received 29 May 2016; published 21 October 2016)

We study the temperature dependence of nuclear magnetic relaxation (NMR) rates to detect unconventional superconductivity in doped topological insulators, such as $M(=\text{Cu,Nb,Sr})_x\text{Bi}_2\text{Se}_3$ and $\text{Sn}_{1-x}\text{In}_x\text{Te}$. The Hebel-Slichter coherence effect below a critical temperature T_c depends on the superconducting states predicted by a minimal model of doped topological insulators. In a nodal anisotropic topological state similar to the ABM phase in ^{3}He, the NMR rate has a conventional s-wave-like coherence peak below T_c. In contrast, in a fully-gapped isotropic topological superconducting state, this rate below T_c exhibits an antipeak profile. Moreover, in a twofold in-plane anisotropic topological superconducting state, there is no coherence effect, which is similar to that in a chiral p-wave state. We also claim in a model of $\text{Cu}_x\text{Bi}_2\text{Se}_3$ that a signal of the fully-gapped odd-parity state is attainable from the change of the antipeak behavior depending on doping level. Thus, we reveal that the NMR rates shed light on unconventional superconductivity in doped topological insulators.

DOI: 10.1103/PhysRevB.94.134516

I. INTRODUCTION

The recent discovery of topological insulators [1–10] leads to a number of studies about topological aspects in condensed matter physics [11]. Topological superconductors have also attracted much attention because of their potential applications for topological quantum computing [12]. The quest for bulk topological superconductors is an exciting issue in topological material science. Both surface and bulk probes are crucial for identifying topological materials. The bulk-boundary correspondence indicates that the presence of gapless surface bound states between different topological materials is an evidence of a nontrivial topological order. Bulk quantities also contain a signature of their topological order. A definite example in condensed matter physics is the conductance in the integer quantum Hall systems [13]. Quantized behaviors ruled by a topological invariant are observed.

Doped topological insulators are candidates of 3D time-reversal invariant topological superconductors with Z_2 invariants [14,15]. Bi_2Se_3 has a superconducting critical temperature T_c around 3 K with Cu, Sr, and Nb doping [16–19]. The doped topological crystalline insulator $\text{Sn}_{1-x}\text{In}_x\text{Te}$ also becomes a superconductor with $T_c \sim 4$ K [20,21]. The properties of $\text{Cu}_x\text{Bi}_2\text{Se}_3$ and $\text{Sn}_{1-x}\text{In}_x\text{Te}$ are studied by different physical probes, including point-contact spectroscopy [20,22,23], scanning tunneling spectroscopy [24], the Knight-shift measurement [25], and the angular-resolved heat capacity measurement [26]. The point-contact spectroscopy showed the zero-bias conductance peaks from the Majorana bound states at the surface edges. The scanning tunneling spectroscopy, however, indicated a fully gapped feature in the density of states; there is no in-gap state, and therefore the superconducting state could be topologically trivial. In addition, the Knight-shift and the angular-resolved heat capacity measurements on $\text{Cu}_x\text{Bi}_2\text{Se}_3$ showed the presence of twofold in-plane anisotropy. This result indicates a strong anisotropic order parameter since the normal-state electronic structure has a sixfold in-plane symmetry caused by the crystal structure [27–30]. A similar anisotropic feature is also observed by the torque magnetometry measurement in $\text{Nb}_x\text{Bi}_2\text{Se}_3$ [19]. Thus, the doped topological insulators have unconventional properties in their superconducting states, which might be topologically nontrivial superconductors.

A correlation function is a key quantity of connecting topological characters with bulk measurements. Current-current correlation functions signal the topological invariant in integer Hall systems as a quantized conductance, for example. In topological superconductors, the authors proposed that spin-spin correlation functions, measured by the nuclear magnetic relaxation (NMR) rate (T_1^{-1}), can detect their topological nature [31]. The NMR rate in a spin-singlet s-wave superconductor is enhanced just below T_c, owing to the coherence factor [32]. This coherence peak (Hebel-Slichter peak) comes from the formation of s-wave-like Cooper pairs [33,34]. We claimed that an inverse coherence effect is the signature of a 3D odd-parity fully gapped topological superconducting state in time-reversal-invariant multiorbital systems; the coherence factor contributes to the NMR rates with an opposite sign to that of the conventional s-wave states.

In this paper, we study the temperature dependence of NMR rates to detect a sign of unconventional topological superconductivity in doped topological insulators $M(=\text{Cu,Nb,Sr})_x\text{Bi}_2\text{Se}_3$ and $\text{Sn}_{1-x}\text{In}_x\text{Te}$. We focus on both isotropic and anisotropic superconducting states. Our model is a massive Dirac Hamiltonian with a superconducting gap. This is a minimal model of 3D time-reversal-invariant multiband topological superconductors. Moreover, we add a hexagonal warping term to the normal-electron Hamiltonian, allowing us to argue an effect of in-plane six-fold symmetry [30]. Focusing on a model of $\text{Cu}_x\text{Bi}_2\text{Se}_3$, we also claim that the disappearance of the inverse coherence effect leads to a signal of the fully-gapped odd-parity state when doping level increases. We reveal that the NMR rate in a 3D doped topological insulator becomes a tool to detect topologically nontrivial unconventional superconductivity, even with the hexagonal warping term.

This paper is organized as follows. Section II shows our mean-field superconducting model of doped topological insulators. We also show the explicit formula of the NMR rate. In Sec. III, we show the approximate formulation of the NMR rate below T_c. In Sec. IV, the numerical results are shown. We discuss the effect of the hexagonal warping term. In Sec. V, we examine the dependence of the coherence effects on electron doping level more closely. Section VI shows the discussion. The summary is given in Sec. VII.

II. MODEL

The mean-field Bogoliubov-de Gennes (BdG) Hamiltonian is $\mathcal{H} = (1/2)\sum_{\boldsymbol{k}} \boldsymbol{\psi}_{\boldsymbol{k}}^{\dagger} \check{H}(\boldsymbol{k}) \boldsymbol{\psi}_{\boldsymbol{k}}$, with $\boldsymbol{\psi}_{\boldsymbol{k}} = (\boldsymbol{c}_{\boldsymbol{k}}^{\dagger}, \boldsymbol{c}_{-\boldsymbol{k}}^{\mathrm{T}})$ and $\boldsymbol{\psi}_{\boldsymbol{k}}^{\mathrm{T}} = (\boldsymbol{c}_{\boldsymbol{k}}, \boldsymbol{c}_{-\boldsymbol{k}}^{\dagger})$. The $2n_{\mathrm{o}}$-component column (raw) vector $\boldsymbol{c}_{\boldsymbol{k}}$ ($\boldsymbol{c}_{\boldsymbol{k}}^{\dagger}$) contains electron's annihilation (creation) operators, with the number of orbitals n_{o}. When $n_{\mathrm{o}} = 2$, we have $\boldsymbol{c}_{\boldsymbol{k}}^{\mathrm{T}} = (c_{\uparrow\boldsymbol{k}}^{1}, c_{\downarrow\boldsymbol{k}}^{1}, c_{\uparrow\boldsymbol{k}}^{2}, c_{\downarrow\boldsymbol{k}}^{2})$. The BdG matrix $\check{H}(\boldsymbol{k})$ is

$$\check{H}(\boldsymbol{k}) = \begin{pmatrix} \hat{H}_0(\boldsymbol{k}) & \hat{\Delta}(\boldsymbol{k}) \\ \hat{\Delta}^{\dagger}(\boldsymbol{k}) & -\hat{H}_0(-\boldsymbol{k})^{*} \end{pmatrix}, \tag{1}$$

where the normal-state Hamiltonian matrix is $\hat{H}_0(\boldsymbol{k})$. The pairing potential fulfills $\hat{\Delta}^{\mathrm{T}}(\boldsymbol{k}) = -\hat{\Delta}(-\boldsymbol{k})$, owing to the Fermion anticommutation property. $\check{A}$ signifies the $2n_{\mathrm{o}} \times 2n_{\mathrm{o}}$ matrix structure in the Nambu-Gor'kov particle-hole space, whereas $\hat{A}$ does the $n_{\mathrm{o}} \times n_{\mathrm{o}}$ matrix structure in the orbital-spin space.

In this paper, we focus on a minimal model for 3D time-reversal-invariant topological superconductor. A typical candidate for a topological superconductor is a doped topological insulator with a strong spin orbit coupling, such as $M_x\mathrm{Bi_2Se_3}$ and $\mathrm{Sn}_{1-x}\mathrm{In}_x\mathrm{Te}$. The low-energy normal-state $\boldsymbol{k}\cdot\boldsymbol{p}$ Hamiltonian around a time-reversal-invariant point in the momentum space (e.g. Γ point in $M_x\mathrm{Bi_2Se_3}$ or L point in $\mathrm{Sn}_{1-x}\mathrm{In}_x\mathrm{Te}$) is given by a massive Dirac Hamiltonian [14,20,22,28,35,36]

$$\hat{H}_0(\boldsymbol{k}) = \gamma^0\left[-\mu\Gamma^0 + \sum_{i=1}^{3} v_i k_i \Gamma^i + m\Gamma^4 + h_5(\boldsymbol{k})\Gamma^5\right], \tag{2}$$

with chemical potential μ, spin-orbit coupling constants v_i, and mass m. This Hamiltonian is the same as that in Ref. [14] except h_5. The last term $h_5(\boldsymbol{k}) \equiv i\lambda(k_+^3 + k_-^3)$ with $k_\pm = k_x \pm ik_y$ corresponds to the effects of hexagonal warping in the Fermi surface of $M_x\mathrm{Bi_2Se_3}$ [30]. Six kinds of 4×4 matrices Γ^A ($A = 0,1\ldots,5$) are composed of the gamma matrices γ^μ ($\mu = 0,1,2,3$) [37] and the identity: $\Gamma^A = \gamma^A$ ($A \neq 4$) and $\Gamma^4 = \mathbb{1}_4$, with $\gamma^5 = i\gamma^0\gamma^1\gamma^2\gamma^3$. Our choice [38] is that $\gamma^0 = \sigma_x \otimes \mathbb{1}_2$, $\gamma^1 = -i\sigma_y \otimes s_y$, $\gamma^2 = i\sigma_y \otimes s_x$, and $\gamma^3 = i\sigma_z \otimes \mathbb{1}_2$, where $\sigma_{x,y,z}$ ($s_{x,y,z}$) are the 2×2 Pauli matrices in the orbital (spin) space. In Sec. V, we argue a more suitable model for studying doped topological insulator $\mathrm{Cu}_x\mathrm{Bi_2Se_3}$. In this paper, we study the momentum-independent pair potential $\hat{\Delta}$, owing to the onsite interaction [14,15]. The fermion anticommutation relation leads to

$$\hat{\Delta}^A = \Delta^A \Gamma^A \gamma^2 \gamma^5. \tag{3}$$

Since $\gamma^2\gamma^5 = \mathbb{1}_2 \otimes s_y$, the case of Γ^A to be the identity (i.e., $A = 4$) describes a spin-singlet s-wave state: $\Delta^4 \propto \sum\langle c_{-\boldsymbol{k}\downarrow}^{1} c_{\boldsymbol{k}\uparrow}^{1} + c_{-\boldsymbol{k}\downarrow}^{2} c_{\boldsymbol{k}\uparrow}^{2}\rangle$. The additional Γ^A ($A \neq 4$) characterizes a *twist* of each order-parameter component in the orbital-spin space, compared to the conventional s-wave state. According to Ref. [14], even-parity order parameters (A_{1g} states) are given by Δ^4 and Δ^0. Odd-parity states correspond to $\Delta^{1,2,3,5}$. The component Δ^5 corresponds to an odd-parity fully-gapped (A_{1u}) state [14,15]: $\Delta^5 \propto \sum\langle c_{-\boldsymbol{k}\downarrow}^{2} c_{\boldsymbol{k}\uparrow}^{1} + c_{-\boldsymbol{k}\uparrow}^{2} c_{\boldsymbol{k}\downarrow}^{1}\rangle$. The others are anisotropic odd-parity topological states; Δ^1 and Δ^2 (E_u states) have deep minima, respectively, in the directions of the x and y axes, whereas Δ^3 (A_{2u} state) does so in the z direction. Specifically, the odd-parity states with twofold deep gap minima on the a-b plane are composed of $\Delta^1 \propto \sum\langle c_{-\boldsymbol{k}\uparrow}^{1} c_{\boldsymbol{k}\uparrow}^{2} - c_{-\boldsymbol{k}\downarrow}^{1} c_{\boldsymbol{k}\downarrow}^{2}\rangle$ and $\Delta^2 \propto \sum\langle c_{-\boldsymbol{k}\uparrow}^{1} c_{\boldsymbol{k}\uparrow}^{2} + c_{-\boldsymbol{k}\downarrow}^{1} c_{\boldsymbol{k}\downarrow}^{2}\rangle$. In the case of E_g pairing without the hexagonal warping term (e.g., $\lambda = 0$), the superconducting order parameter with point nodes in the θ_{N} direction is expressed as [29]

$$\hat{\Delta}_{\theta_{\mathrm{N}}} = (\cos\theta_{\mathrm{N}}\hat{\Delta}^1 + \sin\theta_{\mathrm{N}}\hat{\Delta}^2). \tag{4}$$

The point nodes are located at [29]

$$\boldsymbol{k}_{\mathrm{node}}^{\pm} = \pm\sqrt{\mu^2 - m^2 + |\Delta|^2}(\cos\theta_{\mathrm{N}}, \sin\theta_{\mathrm{N}}, 0). \tag{5}$$

Here, we adopt $|\Delta|^2 = |\Delta^1|^2 = |\Delta^2|^2$. With increasing λ, the point nodes change to the deep minima in the momentum space [30]. In this paper, we set $\theta_{\mathrm{N}} = 0$; the nodes are lifted up by the hexagonal warping term, resulting in a full gap.

The NMR rate [31,39,40] in a multiorbit superconductor is calculated by

$$\frac{1}{T_1(T)T} = \pi \sum_{\alpha,\alpha'} \int_{-\infty}^{\infty} d\omega \left[-\frac{df(\omega)}{d\omega}\right] \times \mathrm{Re}\,\{\rho_{\uparrow\uparrow}^{G\alpha\alpha'}(\omega)\rho_{\downarrow\downarrow}^{G\alpha'\alpha}(\omega) - \rho_{\uparrow\downarrow}^{F\alpha\alpha'}(\omega)[\rho_{\downarrow\uparrow}^{F\alpha\alpha'}(\omega)]^{*}\}. \tag{6}$$

We use the unit system of $\hbar = k_{\mathrm{B}} = 1$. The indices α and α' represent orbital labels. The Fermi-Dirac distribution function is denoted by $f(\omega) = 1/(e^{\omega/T} + 1)$. The spectral functions $\hat{\rho}^G(\omega)$ and $\hat{\rho}^F(\omega)$ are the submatrices of

$$\check{\rho}^G(\omega) = \frac{-1}{2\pi i}\sum_{\boldsymbol{k}}[\check{G}_{\boldsymbol{k}}(i\omega_n \to \omega + i0) - \check{G}_{\boldsymbol{k}}(i\omega_n \to \omega - i0)], \tag{7}$$

with the temperature Green's function defined as

$$\check{G}_{\boldsymbol{k}}(i\omega_n) = [i\omega_n - \check{H}(\boldsymbol{k})]^{-1}. \tag{8}$$

Here, the fermionic Matsubara frequency is $\omega_n = \pi T(2n+1)$ ($n \in \mathbb{Z}$). The matrix form of $\check{G}_{\boldsymbol{k}}(i\omega_n)$ in the Nambu-Gor'kov particle-hole space is

$$\check{G}_{\boldsymbol{k}}(i\omega_n) = \begin{pmatrix} \hat{G}_{\boldsymbol{k}}(i\omega_n) & \hat{F}_{\boldsymbol{k}}(i\omega_n) \\ \hat{\bar{F}}_{\boldsymbol{k}}(i\omega_n) & \hat{\bar{G}}_{\boldsymbol{k}}(i\omega_n) \end{pmatrix}. \tag{9}$$

The diagonal block $\hat{G}_{\boldsymbol{k}}$ leads to $\hat{\rho}^G$, relevant to the electron's density of states. The off-diagonal block $\hat{F}_{\boldsymbol{k}}$ contributes to the anomalous spectral function $\hat{\rho}^F$.

III. APPROXIMATE FORMULATION BELOW T_c

A coherence effect just below T_c originates from the second term in Eq. (6) [39,41]. The Hebel-Slichter peak appears when this term, including the minus sign in front of the spectral functions, has a positive contribution to T_1^{-1}. To understand the behaviors of the second term, we evaluate anomalous Green's function near T_c. Linearizing $\check{G}$ with respect to $\hat{\Delta}^A$, we obtain

$$\hat{F}_{\boldsymbol{k}}^A(i\omega_n) \approx \hat{G}_{\boldsymbol{k}}^{\mathrm{N}}(i\omega_n)\hat{\Delta}^A\hat{\bar{G}}_{\boldsymbol{k}}^{\mathrm{N}}(i\omega_n), \tag{10}$$

with normal-state Green's functions:

$$\hat{G}_{\boldsymbol{k}}^{\mathrm{N}}(i\omega_n) \equiv [i\omega_n - \hat{H}_0(\boldsymbol{k})]^{-1}, \tag{11}$$

$$\hat{\bar{G}}_{\boldsymbol{k}}^{\mathrm{N}}(i\omega_n) \equiv [i\omega_n + \hat{H}_0(-\boldsymbol{k})^*]^{-1}. \tag{12}$$

With the use of the relation $\gamma^2\gamma^5\hat{H}_0(-\boldsymbol{k})^*\gamma^2\gamma^5 = \hat{H}_0(\boldsymbol{k})$, we have

$$\begin{aligned}\hat{\bar{G}}_{\boldsymbol{k}}^{\mathrm{N}}(i\omega_n) &= \gamma^2\gamma^5(i\omega_n + \hat{H}_0(\boldsymbol{k}))^{-1}\gamma^2\gamma^5,\\ &= -\gamma^2\gamma^5\hat{G}_{\boldsymbol{k}}^{\mathrm{N}}(-i\omega_n)\gamma^2\gamma^5.\end{aligned} \tag{13}$$

A normal-state Green's function is evaluated by an algebraic relation of $\hat{H}_0$; we find that $[\hat{H}_0'(\boldsymbol{k})]^2 = E(\boldsymbol{k})^2$, with $\hat{H}_0' \equiv \hat{H}_0 + \mu$ and $E(\boldsymbol{k})^2 = \sum_{i=1}^3 v_i^2 k_i^2 + m^2 - h^5(\boldsymbol{k})^2$. This property corresponds to the fact that the Dirac equation is the square root of the Klein-Gordon equation [37]. Hence, we obtain

$$\hat{G}_{\boldsymbol{k}}^{\mathrm{N}}(i\omega_n) = \sum_{\ell=\pm}\frac{\hat{P}_\ell(\boldsymbol{k})}{i\omega_n - \ell E(\boldsymbol{k}) + \mu}, \tag{14}$$

with the projectors

$$\hat{P}_\pm = \frac{1}{2}\left[1 \pm \frac{\hat{H}_0'}{E(\boldsymbol{k})}\right] \equiv \gamma^0\sum_{A=0}^5 w_{\ell\boldsymbol{k}}^A\Gamma^A. \tag{15}$$

Just below T_c, the anomalous Green's function $\hat{F}_{\boldsymbol{k}}(i\omega_n)$ is expressed as

$$\hat{F}_{\boldsymbol{k}}^A(i\omega_n) = -\sum_{l,l'=\pm} W_{ll'\boldsymbol{k}}(i\omega_n)\hat{P}_l(\boldsymbol{k})\hat{P}_{l'A}(\boldsymbol{k})\hat{\Delta}^A, \tag{16}$$

with

$$W_{ll'\boldsymbol{k}}(i\omega_n) \equiv \frac{1}{i\omega_n - lE(\boldsymbol{k}) + \mu}\frac{1}{-i\omega_n - l'E(\boldsymbol{k}) + \mu}, \tag{17}$$

$$\hat{P}_{l'A}(\boldsymbol{k}) \equiv \Gamma^A\hat{P}_l(\boldsymbol{k})[\Gamma^A]^{-1} \equiv \gamma^0\sum_{A'=0}^5 w_{l\boldsymbol{k}}^{AA'}\Gamma^{A'}. \tag{18}$$

Thus, the local anomalous Green's function becomes

$$\sum_{\boldsymbol{k}} F_{\boldsymbol{k}}^A(i\omega_n) = \alpha_A\hat{\Delta}^A + \beta_A\gamma^0\hat{\Delta}^A + \delta_A\gamma^1\gamma^5\hat{\Delta}^A. \tag{19}$$

Here, we use the fact that momentum-odd terms in $\hat{P}_l(\boldsymbol{k})$ vanish. The coefficients α_A, β_A, and δ_A are defined as

$$\alpha_A(i\omega_n) = -\sum_{\boldsymbol{k}}\sum_{l,l=\pm} W_{ll'\boldsymbol{k}}(i\omega_n)\sum_{A'=0}^5 w_{l\boldsymbol{k}}^{A'}w_{l'\boldsymbol{k}}^{AA'}(1 - 2\delta_{A'5}), \tag{20}$$

$$\beta_A(i\omega_n) = -\sum_{\boldsymbol{k}}\sum_{l,l=\pm} W_{ll'\boldsymbol{k}}(i\omega_n)\left(w_{l\boldsymbol{k}}^4 w_{l'\boldsymbol{k}}^{A0} + w_{l\boldsymbol{k}}^0 w_{l'\boldsymbol{k}}^{A4}\right), \tag{21}$$

$$\delta_A(i\omega_n) = -\sum_{\boldsymbol{k}}\sum_{l,l=\pm} W_{ll'\boldsymbol{k}}(i\omega_n)\left(w_{l\boldsymbol{k}}^5 w_{l'\boldsymbol{k}}^{A1} - w_{l\boldsymbol{k}}^1 w_{l'\boldsymbol{k}}^{A5}\right). \tag{22}$$

The sign of the coherence effect of T_1^{-1} is determined by the spin parity of the local anomalous Green's function [31]. The first and second terms of $\sum_{\boldsymbol{k}} F_{\boldsymbol{k}}^A(i\omega_n)$ in Eq. (19) have the spin parity of the order parameter $\hat{\Delta}^A$, since the multiplication of γ^0 with $\hat{\Delta}^A$ does not change the property of a spin-index exchange. The third term, which is proportional to the warping term h_5, rotates spins, since $\gamma^1\gamma^5 = \mathbb{1}_2 \otimes s_x$. For example, in the case of the fully-gapped odd-parity state $\hat{\Delta}^5 \propto \sigma_y \otimes s_x$, the first and second terms contribute to the anomalous spectral function $\rho_{\uparrow\downarrow}^{\alpha\alpha'} = \rho_{\downarrow\uparrow}^{\alpha\alpha'}$. The third term does not contribute to the anomalous spectral function, since this term is proportional to $\gamma^1\gamma^5\hat{\Delta}^5 \propto \sigma_y \otimes \mathbb{1}_2$. Thus, the inverse coherence effect [31] can appear, irrespective of hexagonal warping. In the case of the anisotropic odd-parity state $\hat{\Delta}^1 \propto \sigma_y \otimes \mathbb{1}_2$, the spin-singlet element of the gap function $\Delta_{\uparrow\downarrow}^{\alpha\alpha'}$ is zero so that the first and second terms do not contribute to the NMR rate. The only third term contributes to $\rho_{\uparrow\downarrow}^{\alpha\alpha'} = \rho_{\downarrow\uparrow}^{\alpha\alpha'}$ and the amplitude of the inverse coherence effect is proportional to the magnitude of the warping term.

IV. NUMERICAL RESULTS

In this section, we show the temperature dependence of the NMR rate T_1^{-1} with various odd-parity superconducting phases. We assume the phenomenological temperature dependence of the gap amplitude as [40]

$$\Delta(T) = \Delta_0\tanh(a\sqrt{T_c/T - 1}), \tag{23}$$

with $T_c = 1.76\Delta_0$. Equation (23) with $a = 1.74$ reproduces well the temperature dependence of the BCS gap. We set the gap amplitude $\Delta_0 = 0.1$, the Dirac mass $m = 0.4$, and the spin-orbit interaction $v_i = 1$. The $\boldsymbol{k}$ integrals are performed by the trapezoidal rule in the spherical coordinate system, with cutoff momentum $k_{\max} = 9$ and mesh $(N_k,N_\phi,N_\theta) = (384,96,96)$. The smearing factor of the delta function is set by 0.01. To compare with the previous results by self-consistently solving the gap equations [31], we set same parameter the with $\mu = 0.8$ as that in Ref. [31]. We introduce the effective gap function on the Fermi surface to discuss the quasiparticle excitations due to the thermal effect. According to Eq. (9) in Ref. [30], the spectral gap on the Fermi surface in the presence of the hexagonal warping in the Δ^1 state is expressed as

$$\Delta^{\mathrm{spec},1}(\boldsymbol{k}) = |\Delta|\sqrt{1 - [\tilde{\boldsymbol{k}}\cdot(\hat{z}\times\boldsymbol{n})]^2}, \tag{24}$$

with $\tilde{\boldsymbol{k}} \equiv (k_x,k_y,k_z)/\sqrt{\mu^2 - m^2}$ and $\boldsymbol{n} = (0,1,0)$.

A. Without the warping term h_5

In this section, we drop the warping term h_5. The Fermi surface in normal states is isotropic as shown in Fig. 1(a). Dropping the warping term, there are point nodes in the x direction in the Δ^1 state. The results are summarized as Table I.

Figure 2 shows the temperature dependence of the NMR rate with various kinds of gap functions. First, let us argue the results of the isotropic gaps [Figs. 2(a) and 2(b)]. Just below T_c we confirm the coherence effects predicted in Sec. III. We find a standard behavior in the low-temperature region, caused by a full gap. We stress that all of the non-self-consistent

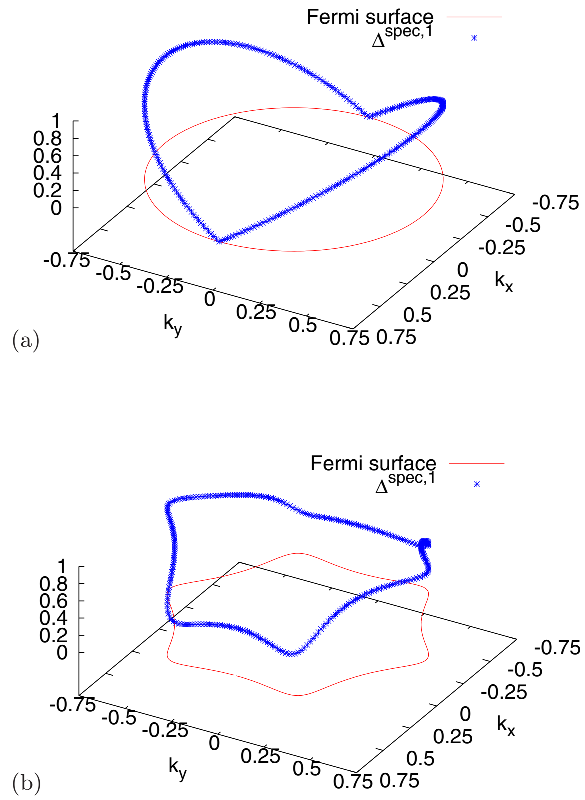

FIG. 1. The Fermi surface and the spectral gap $\Delta^{\rm spec,1}(\boldsymbol{k})$ defined in Eq. (24) with $k_z = 0$ (a) without and (b) with the hexagonal warping term ($\lambda = 1$) to treat the sixfold crystal structure.

TABLE I. Parity table of different gap functions. The coherence effect is characterized by spin parity $p_{\rm s}$ $[\Delta^{\alpha\alpha'}_{\uparrow\downarrow}(\boldsymbol{k}) = p_{\rm s}\Delta^{\alpha\alpha'}_{\downarrow\uparrow}(\boldsymbol{k})]$, momentum parity $p_{\rm m}$ $[\Delta^{\alpha\alpha'}_{\uparrow\downarrow}(\boldsymbol{k}) = p_{\rm m}\Delta^{\alpha\alpha'}_{\uparrow\downarrow}(-\boldsymbol{k})]$, and orbital parity $p_{\rm o}$ $[\Delta^{\alpha\alpha'}_{\uparrow\downarrow}(\boldsymbol{k}) = p_{\rm o}\Delta^{\alpha'\alpha}_{\uparrow\downarrow}(\boldsymbol{k})]$, with $p_{\rm s}p_{\rm m}p_{\rm o} = -1$.

Gap type	Spin parity $p_{\rm s}$	Orbital parity $p_{\rm o}$	Anisotropic direction	Coherence effect
$A_{1g}(\Delta^4)$ state	-1	$+1$	Isotropic	positive
$A_{1u}(\Delta^5)$ state	$+1$	-1	Isotropic	negative
$A_{2u}(\Delta^3)$ state	-1	$+1$	z	positive
$E_u(\Delta^1$ or $\Delta^2)$ state	$+1$	-1	x or y	negligible negative

temperature dependences have a good qualitative agreement with those in our previous self-consistent calculations [31]. It indicates that the usage of Eq. (23) is adequate for investigating the temperature dependence of the NMR rates in doped topological insulators.

Next we focus on the anisotropic topological states. As shown in Fig. 2(c), the positive coherence effect appears in the $\hat{\Delta}^3$ state, since the spin parity of the gap function $\hat{\Delta}^3 \propto \sigma_z \otimes s_y$ is odd so that the anomalous spectral function becomes $\rho^{\alpha\alpha'}_{\uparrow\downarrow} = -\rho^{\alpha\alpha'}_{\downarrow\uparrow}$. In the case of the $\hat{\Delta}^1$ state, as shown in Fig. 2(d), no coherence effect occurs. As discussed in Sec. III, this gap function without the warping term h_5 does not have spin-off-diagonal elements of the anomalous spectral function (i.e., $\rho^{\alpha\alpha'}_{\uparrow\downarrow} = \rho^{\alpha\alpha'}_{\downarrow\uparrow} = 0$). In the low-temperature region ($T \sim 0.2T_{\rm c}$), there are low-energy quasiparticle excitations in Figs. 2(c) and

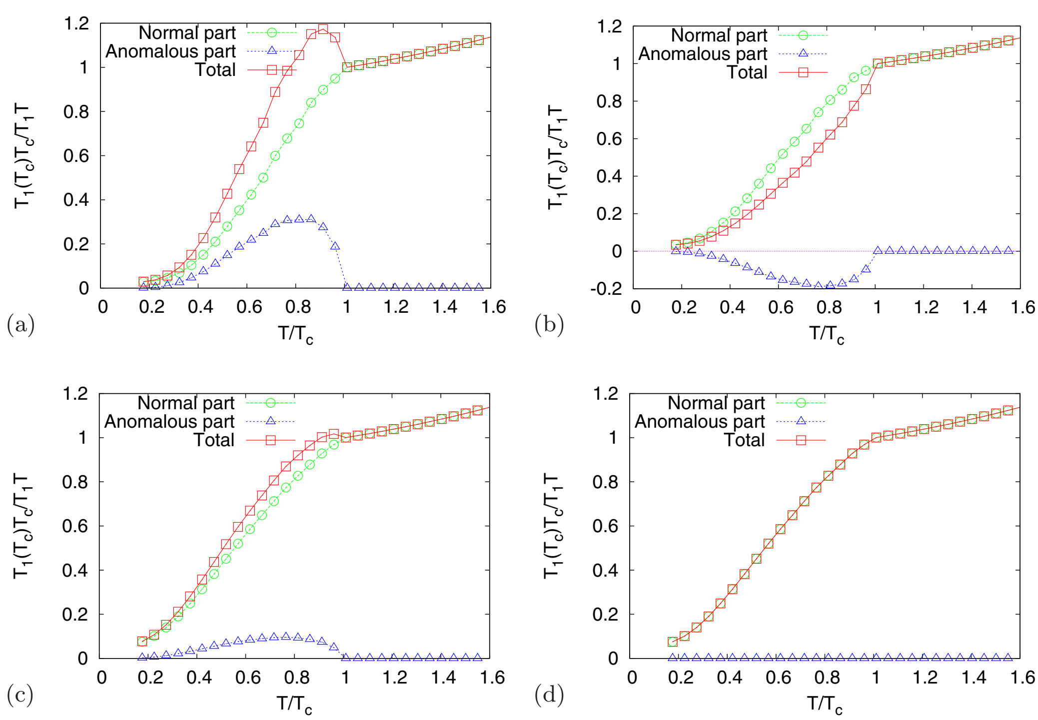

FIG. 2. Temperature dependence of nuclear magnetic relaxation rates in (a) an even-parity gap Δ^4 $(A_{1g}) \propto \sum\langle c^1_{-k\downarrow}c^1_{k\uparrow} + c^2_{-k\downarrow}c^2_{k\uparrow}\rangle$, a fully-gapped isotropic odd-parity gap Δ^5 $(A_{1u}) \propto \sum\langle c^2_{-k\downarrow}c^1_{k\uparrow} + c^2_{-k\uparrow}c^1_{k\downarrow}\rangle$, (c) a nodal odd-parity gap Δ^3 $(A_{2u}) \propto \sum\langle c^1_{-k\downarrow}c^1_{k\uparrow} - c^2_{-k\downarrow}c^2_{k\uparrow}\rangle$, and (d) a nodal odd-parity gap Δ^1 $(E_u) \propto \sum\langle c^1_{-k\uparrow}c^2_{k\uparrow} - c^1_{-k\downarrow}c^2_{k\downarrow}\rangle$. We set the chemical potential $\mu = 0.8$, the Dirac mass $m = 0.4$, and the gap amplitude $\Delta_0 = 0.01$. We ignore the warping term. Equation (23) is used as the phenomenological temperature dependence of the gap amplitude.

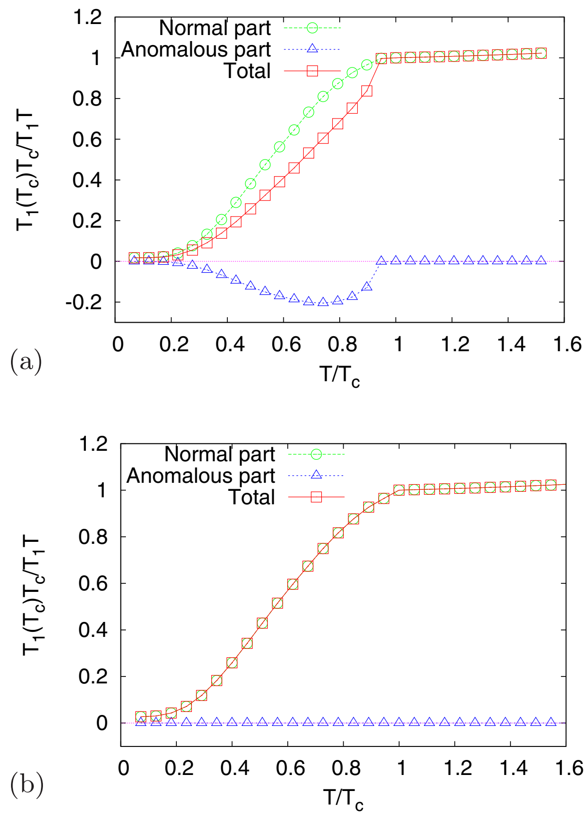

FIG. 3. Temperature dependence of nuclear magnetic relaxation rates with the hexagonal warping term in (a) a fully-gapped isotropic odd-parity gap Δ^5 (A_{1u}) and (b) an anisotropic odd-parity gap Δ^1 (E_u). The parameters are the same as in Fig. 2.

2(d), since $\hat{\Delta}^3$ (A_{2u}) and $\hat{\Delta}^1$ (E_u) states have point nodes in momentum space.

B. With the warping term h_5

We take the warping term h_5 into account to consider a sixfold symmetry due to the crystal structure. We consider $\lambda = 1$ to describe an anisotropic Fermi surface. The Fermi surface with the warping term is shown in Fig. 1(b). On this Fermi surface, the spectral gap function $\Delta^{\mathrm{spec},1}(\boldsymbol{k})$ does not have point nodes.

In both $\Delta^5(A_{1u})$ and $\Delta^1(E_u)$ states, the warping term slightly changes the temperature dependence of the NMR rate, as shown in Fig. 3. The difference between Fig. 2(a) and Fig. 3(a) with the Δ^5 gap function comes from the density of states on the Fermi surface, since the third term in Eq. (19), induced by the warping term, does not contribute to the NMR rate. In the case of the Δ^1 gap function, an inverse coherence effect induced by the warping term may occur, according to Sec. III. The numerical calculation can conclude, however, that the induced coherence effect is negligibly small as shown in Fig. 3(b). We confirm that the relativistic indicator, introduced in Ref. [31], does not affect the induced coherence effect, by changing the Dirac mass m and the chemical potential μ. This result comes from the fact that the warping term is the third order of the momentum so that the summation in the whole momentum space becomes small.

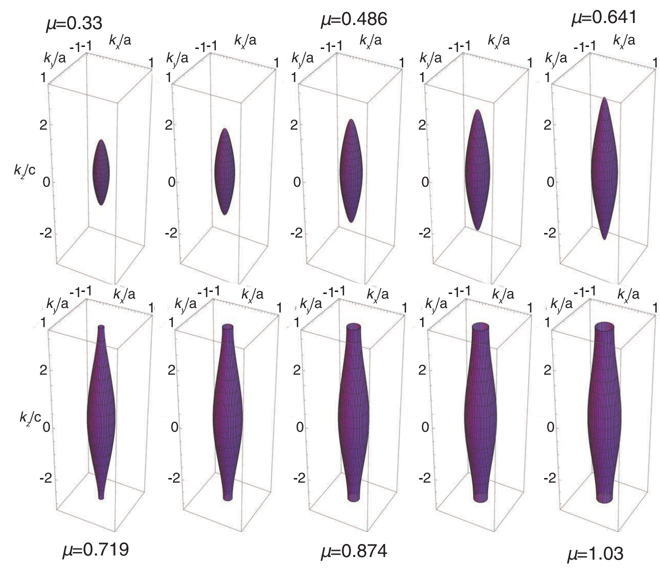

FIG. 4. Doping dependence of the Fermi surface in the model for $Cu_xBi_2Se_3$. The unit of the energy is eV.

At the low temperature region ($T < 0.2T_c$), the amplitude of $1/T_1T$ in Fig. 3(b) is smaller than that in Fig. 2(d). This originates from the fact that there is no point node in the Δ^1 state with the warping term as shown in Fig. 1(b). Note that this difference might be too small to identify whether there are point nodes or not at low temperatures. By comparison with the numerical results with and without the warping term, we conclude that the warping term does not affect the temperature dependence of the NMR rate near T_c.

V. DOPING DEPENDENCE IN THE MODEL FOR $Cu_xBi_2Se_3$

We study the behavior of the coherence peak with respect to the electron doping level in a doped topological insulator $Cu_xBi_2Se_3$. We take a normal-electron model for $Cu_xBi_2Se_3$. According to Ref. [20], we have

$$\hat{H}_0(\boldsymbol{k}) = \gamma^0\left[\varepsilon(\boldsymbol{k})\Gamma^0 + \sum_{i=1}^{3} P_i(\boldsymbol{k})\Gamma^i + P_4(\boldsymbol{k})\Gamma^4\right]. \tag{25}$$

The momentum dependence of the coefficients is summarized as follows [20]: $\varepsilon(\boldsymbol{k}) = \bar{D}_1[2 - 2\cos(k_z c)] + (4\bar{D}_2/3)[3 - 2\cos(\sqrt{3}k_x a/2)\cos(k_y a/2) - \cos(k_y a)] - \mu$, $P_1(\boldsymbol{k}) = (2\bar{A}_2/3)\sqrt{3}\sin(\sqrt{3}k_x a/2)\cos(k_y a/2)$, $P_2(\boldsymbol{k}) = (2\bar{A}_2/3)[\cos(\sqrt{3}k_x a/2)\sin(k_y a/2) + \sin(k_y a)]$, $P_3(\boldsymbol{k}) = \bar{A}_1\sin(k_z c)$, and $P_4(\boldsymbol{k}) = M - \bar{B}_1[2 - 2\cos(k_z c)] - (4\bar{B}_2/3)[3 - 2\cos(\sqrt{3}k_x a/2)\cos(k_y a/2) - \cos(k_y a)]$, with $\bar{D}_2$, $\bar{B}_1$, $\bar{B}_2$, $\bar{A}_2$, and $\bar{A}_1$, determined by first-principles band-structure calculations of Bi_2Se_3 [42]. Taking $|\boldsymbol{k}| \to 0$, we can obtain a linearized massive Dirac Hamiltonian equal to Eq. (2) without the hexagonal warping term. We stress that the algebraic structure of Eq. (25) is the same as that of Eq. (2). Consequently, all the techniques in Sec. III are applicable to the analyses in this section.

We describe the change of doping level via the variation of μ, with keeping $M = 0.28$ eV and $\Delta_0 = 0.05$ eV. Figure 4 shows the doping dependence of the Fermi surface. With

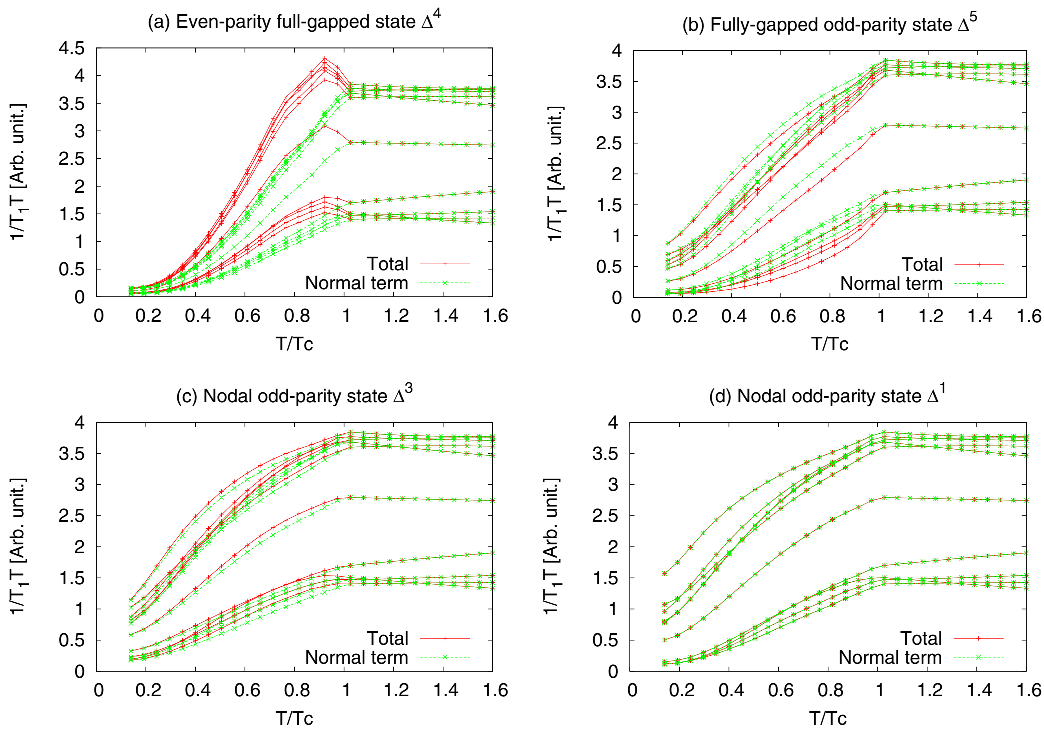

FIG. 5. Temperature dependence of nuclear magnetic relaxation rates in the model for $Cu_xBi_2Se_3$ with (a) an even-parity gap Δ^4 (A_{1g}) $\propto \sum\langle c^1_{-k\downarrow}c^1_{k\uparrow} + c^2_{-k\downarrow}c^2_{k\uparrow}\rangle$, a fully-gapped isotropic odd-parity gap Δ^5 (A_{1u}) $\propto \sum\langle c^2_{-k\downarrow}c^1_{k\uparrow} + c^2_{-k\uparrow}c^1_{k\downarrow}\rangle$, (c) a nodal odd-parity gap Δ^3 (A_{2u}) $\propto \sum\langle c^1_{-k\downarrow}c^1_{k\uparrow} - c^2_{-k\downarrow}c^2_{k\uparrow}\rangle$, and (d) a nodal odd-parity gap Δ^1 (E_u) $\propto \sum\langle c^1_{-k\uparrow}c^2_{k\uparrow} - c^1_{-k\downarrow}c^2_{k\downarrow}\rangle$. The model parameters are shown in Eq. (25). The doping dependence is considered as the chemical potential dependence μ. The minimum and maximum values of the chemical potentials are $\mu = 0.33$ [eV] and $\mu = 1.03$ [eV], respectively. At a higher doping level, larger $(T_1T)^{-1}$ at $T > T_c$. We set the gap amplitude $\Delta_0 = 0.05$ [eV]. Equation (23) is used as the phenomenological temperature dependence of the gap amplitude.

increasing of the doping level, the ellipsoidal Fermi surface changes into the cylindrical Fermi surfaces; it indicates the presence of the Lifshitz transition [43].

Figure 5 shows the NMR rates with different values of μ, depending on the kinds of gap functions. Note that at a higher doping level, larger $(T_1T)^{-1}$ at $T > T_c$. When increasing the doping level, the inverse coherence effect in the fully-gapped odd-parity state Δ^5 (A_{1u}) becomes faint [Fig. 5(b)]. This is contrast to the even-parity state Δ^4 (A_{1g}); the conventional coherence peak is pronounced [Fig. 5(a)]. We also find that the other two states do not significantly depend on the doping level, except for the amount of the normal-state component. Thus, we obtain an interesting way of distinguishing Δ^5 with the others; the disappearance of the inverse coherence effect associated with the increase of the doping level definitely signals the fully-gapped odd-parity state.

We discuss the importance of a multiorbital feature in $Cu_xBi_2Se_3$, before closing this section. A theoretical study on the NMR rate of $Cu_xBi_2Se_3$ with the odd-parity states was reported in Ref. [43]; there was no inverse coherence peak and doping dependence shown in this paper. The discrepancy of the present paper with Ref. [43] is the NMR-rate formula; the NMR rate in a single-band superconductor was utilized there [See Eq. (12) in Ref. [43]]. Thus, the two-orbital character of $Cu_xBi_2Se_3$ is strongly linked to the exotic behaviors of the NMR rate. It is interesting to examine when a single-band approximation is valid. In the case of the massive Dirac Hamiltonian, the condition is obtained intuitively; a lower Dirac band, corresponding to the negative-frequency solution of the free-particle Dirac equation, is negligible in a nonrelativistic limit (i.e., $M \gg k_F^2$) [31]. In contrast, a more realistic model of $Cu_xBi_2Se_3$ given by Eq. (25) has no definite criterion of dropping a specific normal-electron band since the Fermi surfaces are composed of the two orbitals for arbitrary μ.

VI. DISCUSSION

We discuss the amplitude of the coherence effects. As we discussed in Ref. [31], the relativistic indicator defined by $\beta \equiv \sqrt{(\mu/m)^2 - 1}$ characterizes the amplitude of the coherence factor. This indicator is controlled by the chemical potential shift. With increasing the chemical potential μ, the indicator β increases. In the ultrarelativistic limit $\beta \to \infty$ (i.e., either $\mu \to \infty$ or $m \to 0$), the amplitude of the coherence effect becomes largest in the fully-gapped isotropic topological superconducting state Δ^5 (A_{1u}), as shown in Fig. 3 in Ref. [31]. We confirm that the similar behaviors occur in other topologically nontrivial superconducting states A_{2u} and E_u.

The robustness of the coherence effect against impurities is important information to measure the NMR rate in experiments. We discussed the robustness of the density of states against impurities in Refs. [44,45]. We concluded that the relativistic indicator β characterizes the impurity effect. In the nonrelativistic limit $\beta \to 0$ (i.e. $\mu \to m$), the topological superconducting states A_{1u} and E_u are fragile against nonmagnetic impurities, since the effective gap functions are p-wave ones [45,46]. In this limit, the Dirac-BdG Hamiltonian is regarded to the BdG Hamiltonian. As we discussed above, the amplitude of the coherence effects in these topological states is proportional to the indicator β so that one does not observe the coherence effects below T_c even without impurities. On the other hand, the low-energy density of states is robust against nonmagnetic impurities in the ultrarelativistic limit. In this limit, the Dirac-BdG equations are divided into a left-handed sector and a right-handed sector as discussed in Ref. [31]. The effective gap functions are s-wave ones. Thus, the large amplitude of the coherence effect is robust against nonmagnetic impurities. We reveal that the NMR rate in a 3D doped topological insulator becomes a tool to detect topologically nontrivial unconventional superconductivity.

VII. SUMMARY

In conclusion, we studied the temperature dependence of the NMR rate in topologically nontrivial superconducting states in doped topological insulators. We found that an inverse coherence effect occurs in a fully-gapped isotropic odd-parity state and a negligible small inverse coherence effect occurs in a strong in-plane anisotropic odd-parity state. The hexagonal warping term to describe the sixfold crystal structure does not affect the temperature dependence of the NMR rate near T_c. At the low temperature region ($T < 0.2T_c$), the amplitude of $1/T_1T$ with the warping term is smaller than that without the warping term. However, this difference might be too small to identify whether there are point nodes or not at low temperatures. We also studied the behavior of the coherence peak with respect to the electron doping level in a doped topological insulator $Cu_xBi_2Se_3$ with the use of the realistic model proposed by the first-principles calculation. The disappearance of the negative coherence effect associated with the increase of the doping level definitely signals the fully-gapped odd-parity state. We reveal that the NMR rate in a 3D doped topological insulator becomes a tool to detect topologically nontrivial unconventional superconductivity.

ACKNOWLEDGMENTS

The authors would like to acknowledge Hiroki Nakamura and Masahiko Machida for helpful discussions and comments. The calculations were performed by the supercomputing system SGI ICE X at the Japan Atomic Energy Agency. This study was partially supported by JSPS KAKENHI Grant No. 26800197 and the Topological Materials Science (No. 16H00995) KAKENHI on Innovative Areas from JSPS of Japan.

[1] B. A. Bernevig, T. L. Hughes, and S.-C. Zhang, Quantum spin Hall effect and topological phase transition in HgTe quantum wells, Science **314**, 1757 (2006).

[2] Y. L. Chen, Z. K. Liu, J. G. Analytis, J.-H. Chu, H. J. Zhang, B. H. Yan, S.-K. Mo, R. G. Moore, D. H. Lu, I. R. Fisher, S. C. Zhang, Z. Hussain, and Z.-X. Shen, Single Dirac Cone Topological Surface State and Unusual Thermoelectric Property of Compounds from a New Topological Insulator Family, Phys. Rev. Lett. **105**, 266401 (2010).

[3] L. Fu and C. L. Kane, Topological insulators with inversion symmetry, Phys. Rev. B **76**, 045302 (2007).

[4] L. Fu, C. L. Kane, and E. J. Mele, Topological Insulators in Three Dimensions, Phys. Rev. Lett. **98**, 106803 (2007).

[5] C. L. Kane and E. J. Mele, Z_2 Topological Order and the Quantum Spin Hall Effect, Phys. Rev. Lett. **95**, 146802 (2005).

[6] M. König, S. Wiedmann, C. Brüne, A. Roth, H. Buhmann, L. W. Molenkamp, X.-L. Qi, and S.-C. Zhang, Quantum spin Hall insulator state in HgTe quantum wells, Science **318**, 766 (2007).

[7] K. Kuroda, M. Ye, A. Kimura, S. V. Eremeev, E. E. Krasovskii, E. V. Chulkov, Y. Ueda, K. Miyamoto, T. Okuda, K. Shimada, H. Namatame, and M. Taniguchi, Experimental Realization of a Three-Dimensional Topological Insulator Phase in Ternary Chalcogenide $TlBiSe_2$, Phys. Rev. Lett. **105**, 146801 (2010).

[8] J. E. Moore and L. Balents, Topological invariants of time-reversal-invariant band structures, Phys. Rev. B **75**, 121306 (2007).

[9] A. Nishide, A. A. Taskin, Y. Takeichi, T. Okuda, A. Kakizaki, T. Hirahara, K. Nakatsuji, F. Komori, Y. Ando, and I. Matsuda, Direct mapping of the spin-filtered surface bands of a three-dimensional quantum spin Hall insulator, Phys. Rev. B **81**, 041309 (2010).

[10] T. Sato, K. Segawa, H. Guo, K. Sugawara, S. Souma, T. Takahashi, and Y. Ando, Direct Evidence for the Dirac-Cone Topological Surface States in Ternary Chalcogenide $TlBiSe_2$, Phys. Rev. Lett. **105**, 136802 (2010).

[11] M. Z. Hasan and C. L. Kane, *Colloquium*: Topological insulators, Rev. Mod. Phys. **82**, 3045 (2010).

[12] J. C. Y. Teo and C. L. Kane, Majorana Fermions and Non-Abelian Statistics in Three Dimensions, Phys. Rev. Lett. **104**, 046401 (2010).

[13] *The Quantum Hall Effect*, 2nd ed., edited by R. E. Prange and S. M. Girvin (Springer, New York, 1990).

[14] L. Fu and E. Berg, Odd-Parity Topological Superconductors: Theory and Application to $Cu_xBi_2Se_3$, Phys. Rev. Lett. **105**, 097001 (2010).

[15] M. Sato, Topological odd-parity superconductors, Phys. Rev. B **81**, 220504(R) (2010).

[16] Y. S. Hor, A. J. Williams, J. G. Checkelsky, P. Roushan, J. Seo, Q. Xu, H. W. Zandbergen, A. Yazdani, N. P. Ong, and R. J. Cava, Superconductivity in $Cu_xBi_2Se_3$ and its Implications for Pairing in the Undoped Topological Insulator, Phys. Rev. Lett. **104**, 057001 (2010).

[17] S. V. K. Maurya, P. Neha, P. Srivastava, and S. Patnaik, Superconductivity by Sr intercalation in the layered topological insulator Bi_2Se_3, Phys. Rev. B **92**, 020506 (2015).

[18] C. Q. Han, H. Li, W. J. Chen, Fengfeng Zhu, Meng-Yu Yao, Z. J. Li, M. Wang, Bo F. Gao, D. D. Guan, Canhua Liu, C. L. Gao, Dong Qian, and Jin-Feng Jia, Electronic structure of a superconducting topological insulator Sr-doped Bi_2Se_3, Appl. Phys. Lett. **107**, 171602 (2015).

[19] T. Asaba, B. J. Lawson, C. Tinsman, L. Chen, P. Corbae, G. Li, Y. Qiu, Y. S. Hor, L. Fu, and L. Li, Rotational symmetry breaking in a trigonal superconductor Nb-doped Bi_2Se_3, arXiv:1603.04040.

[20] S. Sasaki, Z. Ren, A. A. Taskin, K. Segawa, L. Fu, and Y. Ando, Odd-Parity Pairing and Topological Superconductivity in a Strongly Spin-Orbit Coupled Semiconductor, Phys. Rev. Lett. **109**, 217004 (2012).

[21] R. D. Zhong, J. A. Schneeloch, X. Y. Shi, Z. J. Xu, C. Zhang, J. M. Tranquada, Q. Li, and G. D. Gu, Optimizing the superconducting transition temperature and upper critical field of $Sn_{1-x}In_xTe$, Phys. Rev. B **88**, 020505(R) (2013).

[22] S. Sasaki, M. Kriener, K. Segawa, K. Yada, Y. Tanaka, M. Sato, and Y. Ando, Topological Superconductivity in $Cu_xBi_2Se_3$, Phys. Rev. Lett. **107**, 217001 (2011).

[23] T. Kirzhner, E. Lahoud, K. B. Chaska, Z. Salman, and A. Kanigel, Point-contact spectroscopy of $Cu_{0.2}Bi_2Se_3$ single crystals, Phys. Rev. B **86**, 064517 (2012).

[24] N. Levy, T. Zhang, J. Ha, F. Sharifi, A. A. Talin, Y. Kuk, and J. A. Stroscio, Experimental Evidence for s-Wave Pairing Symmetry in Superconducting $Cu_xBi_2Se_3$ Single Crystals Using a Scanning Tunneling Microscope, Phys. Rev. Lett. **110**, 117001 (2013).

[25] K. Matano, M. Kriener, K. Segawa, Y. Ando, and Guo-qing Zheng, Spin-rotation symmetry breaking in the superconducting state of $Cu_xBi_2Se_3$, Nat. Phys. **12**, 852 (2016).

[26] S. Yonezawa, K. Tajiri, S. Nakata, Y. Nagai, Z. Wang, K. Segawa, Y. Ando, and Y. Maeno, Thermodynamic evidence for nematic superconductivity in $Cu_xBi_2Se_3$, Nat. Phys. (2016), doi:10.1038/nphys3907.

[27] T. Hashimoto, K. Yada, A. Yamakage, M. Sato, and Y. Tanaka, Bulk electronic state of superconducting topological insulator, J. Phys. Soc. Jpn. **82**, 044704 (2013).

[28] Y. Nagai, H. Nakamura, and M. Machida, Rotational isotropy breaking as proof for spin-polarized Cooper pairs in the topological superconductor $Cu_xBi_2Se_3$, Phys. Rev. B **86**, 094507 (2012).

[29] Y. Nagai, Field-angle-dependent low-energy excitations around a vortex in the superconducting topological insulator $Cu_xBi_2Se_3$, J. Phys. Soc. Jpn. **83**, 063705 (2014).

[30] L. Fu, Odd-parity topological superconductor with nematic order: Application to $Cu_xBi_2Se_3$, Phys. Rev. B **90**, 100509(R) (2014).

[31] Y. Nagai, Y. Ota, and M. Machida, Inverse coherence effects in nuclear magnetic relaxation rates as a sign of topological superconductivity, Phys. Rev. B **92**, 180502(R) (2015).

[32] M. Tinkham, *Introduction to Superconductivity*, 2nd ed. (Dover, New York, 2004), Chap. 3.

[33] L. C. Hebel and C. P. Slichter, Nuclear spin relaxation in normal and superconducting aluminum, Phys. Rev. **113**, 1504 (1959).

[34] Y. Masuda and A. G. Redfield, Nuclear spin-lattice relaxation in superconducting aluminum, Phys. Rev. **125**, 159 (1962).

[35] T. H. Hsieh, H. Lin, J. Liu, W. Duan, A. Bansil, and L. Fu, Topological crystalline insulators in the SnTe material class, Nat. Commun. **3**, 982 (2012).

[36] Y. Nagai, H. Nakamura, and M. Machida, Spin-polarized Majorana bound states inside a vortex core in topological superconductors, J. Phys. Soc. Jpn. **83**, 064703 (2014).

[37] M. E. Peskin and D. V. Schroeder, *An Introduction to Quantum Field Theory* (Westview Press, Boulder, 1995), Chap. 3.

[38] Our choice is related to the Dirac representation γ_{D}^i by $\gamma^i = \hat{P}\gamma_{\mathrm{D}}^i\hat{P}^\dagger$ with $\hat{P}_{11} = s_0$, $\hat{P}_{12} = -is_z$, $\hat{P}_{21} = s_0$, and $\hat{P}_{22} = is_z$. s_0 is a unit matrix in spin space.

[39] N. Hayashi, K. Wakabayashi, P. A. Frigeri, and M. Sigrist, Nuclear magnetic relaxation rate in a noncentrosymmetric superconductor, Phys. Rev. B **73**, 092508 (2006).

[40] Y. Nagai, N. Hayashi, N. Nakai, H. Nakamura, M. Okumura, and M. Machida, Nuclear magnetic relaxation and superfluid density in Fe-pnictide superconductors: an anisotropic $\pm s$-wave scenario, New J. Phys. **10**, 103026 (2008).

[41] M. Sigrist and K. Ueda, Phenomenological theory of unconventional superconductivity, Rev. Mod. Phys. **63**, 239 (1991).

[42] H. Zhang, C.-X. Liu, X.-L. Qi, X. Dai, Z. Fang, and S.-C. Zhang, Topological insulators in Bi_2Se_3, Bi_2Te_3 and Sb_2Te_3 with a single Dirac cone on the surface, Nat. Phys. **5**, 438 (2009).

[43] T. Hashimoto, K. Yada, A. Yamakage, M. Sato, and Y. Tanaka, Effect of Fermi surface evolution on superconducting gap in superconducting topological insulator, Supercond. Sci. Technol. **27**, 104002 (2014).

[44] Y. Nagai, Y. Ota, and M. Machida, Nonmagnetic impurity effects in a three-dimensional topological superconductor: From p- to s-wave behaviors, Phys. Rev. B **89**, 214506 (2014).

[45] Y. Nagai, Robust superconductivity with nodes in the superconducting topological insulator $Cu_xBi_2Se_3$: Zeeman orbital field and nonmagnetic impurities, Phys. Rev. B **91**, 060502 (2015).

[46] Y. Nagai, H. Nakamura, and M. Machida, Quasiclassical treatment and odd-parity/triplet correspondence in topological superconductors, J. Phys. Soc. Jpn. **83**, 053705 (2014).